ON THE DESIGN OF THE CENTRAL REGION OF AN 8 MeV INJECTOR CYCLOTRON

S.J. Burger, Z.B. du Toit, P.J. Celliers, G.S.Z. Guasco, L.M.M. Roels, H.A. Smit
National Accelerator Centre, CSIR, P.O. Box 72, FAURE, 7131, REPUBLIC OF SOUTH AFRICA

Summary

The optimization of the central region of the k=8 injector cyclotron at the NAC, employing measured magnetic fields and electrolytic tank modelled rf fields, is discussed. An assessment is made of the resultant axial focusing, as well as the axial- and radial acceptance.

1. Introduction

The NAC k=8 Solid-Pole Cyclotron (SPC1) is a four-sector AVF machine with two 90° dees. Operation on harmonic numbers 2 and 6, dee voltages up to 60 kV, and three Constant Geometry Orbits (CGO's) are required to accommodate the desired energy ranges and beam currents of light ions and light heavy ions.[1,2]

The formalism due to M Reiser[3] was used in initial studies. Preliminary design parameters for the central region of SPC1 were then determined by orbit calculations utilising numerically calculated isochronous magnetic fields. The rf fields were derived from measurements on resistance paper and from analytic models. In the final design calculations, measured magnetic fields were used with rf fields derived from measurements on a 3:1 scale model in an electrolytic tank.

2. Layout of the Central Region

Fig. 1 is a schematic representation of the central region of SPC1. The hooded-arc ion source I is of the Livingstone-Jones type, and can be positioned by remote control for each CGO. In position for CGO1, the source is fitted with two winglike protuberances in order to narrow the gaps between the source head and the dummy-dee lips, minimising the deformation of the electric field on the 5th gap crossing on CGO1. The water-cooled puller P has a slit and separate channel for each of the CGO's. Provision is made for initial translational and rotational optimization of the puller orientation, and remote linear adjustment between CGO positions. Two of the three differential probes PR are shown at maximum inward extension. The radial position and width of the two radial (momentum) selecting slits RS are remotely adjustable. The first axial slit AS1 is coupled to RS1 radially, and has a remotely adjustable axial extent. The second axial (phase) selecting slit lies outside the figure. The slit combination RS1/AS1 intercepts the beam on the first turn for CGO2 and CGO3, but on the second turn of CGO1, owing to lack of space.

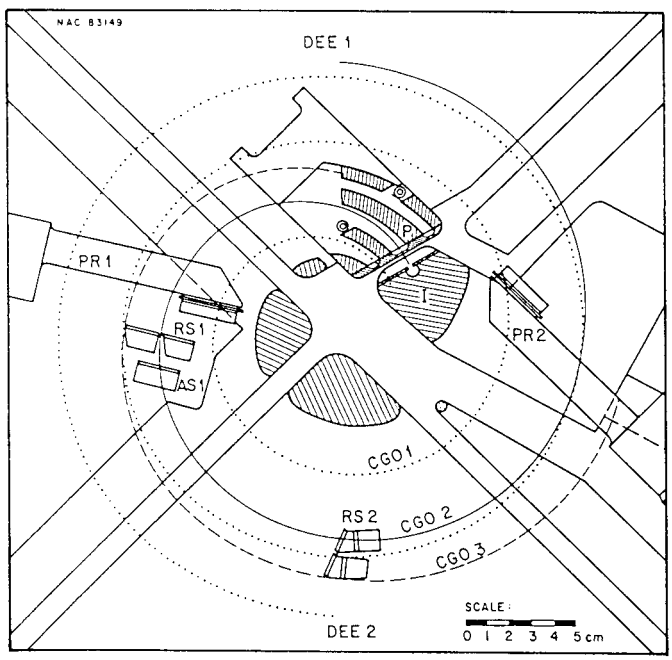

Fig. 1 Layout of the central region of SPC1. The ion source I and puller P are shown in position for the second of the three Constant Geometry Orbits (CGO). Also shown are the radial slits RS, the first axial slit AS and two probes PR.

3. Magnetic and Rf Fields

The measurement and handling of the magnetic field data, as well as the generation and interpolation of isochronous fields, are described elsewhere.[4] Fourier analyses were made of the required fields for input to the orbit code OC[5]. A total of 60 harmonic components were taken into account at each radial value, and were calculated for radii ranging from 0 to 580 mm in 10 mm increments.

In the orbit calculations, the three CGO's are characterised by respectively:-

i) 8 MeV protons - the high-energy beam, variable from 4 to 8 MeV at 10 μA, and with emittance values $\varepsilon_x = \varepsilon_z = 12\pi$ mm.mrad at extraction; extraction radius 0.476 m,

ii) 4 MeV protons - the high-intensity beam, variable from 2 to 4 MeV, at 100 μA, and with emittance values $\varepsilon_x = \varepsilon_z = 38\pi$ mm.mrad at extraction,

iii) 6 MeV $^{12}C^{3+}$ - the light heavy-ion beam and the low-energy light ion beam CGO.

To optimize the ion source position for CGO3 using an essentially flat magnetic field in the central region, it was found necessary to cut away a substantial part of dee 1 on the outer side of the puller at the start of the second turn of CGO1. The alternatives of having either adjustable or demountable dee lips were not acceptable, owing to space limitations and long machine down-time, respectively. To alleviate this problem, we decided to use isochronized magnetic fields with superimposed central cones. The radial shapes of these fields are illustrated in fig. 2. The addition of a cone to the field not only results in rotating the ion source position by 4° in the required direction, but also aids the axial focusing in the central region . The introduction of a central cone however implies that the field in this region will no longer be isochronous, and one does have to take into account the effect on the particle phases. In fig. 3 the phase history of

CH1996-3/84/0000-067 $1.00 © 1984 IEEE

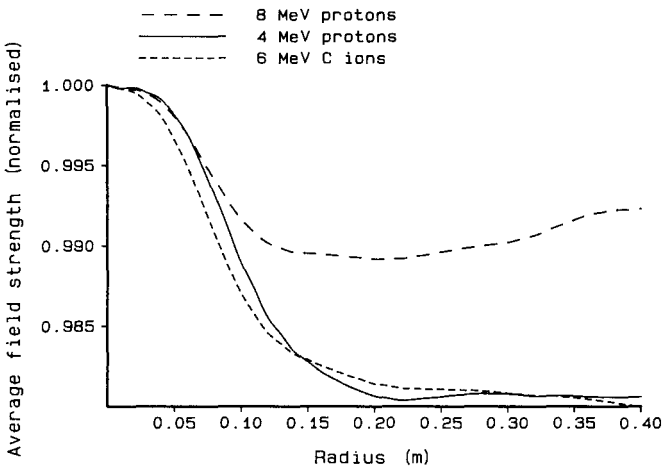

Fig. 2 Radial shapes of the isochronized, measured magnetic fields, with superimposed central cones, used in orbit calculations for the ions characterising the three constant geometry orbits.

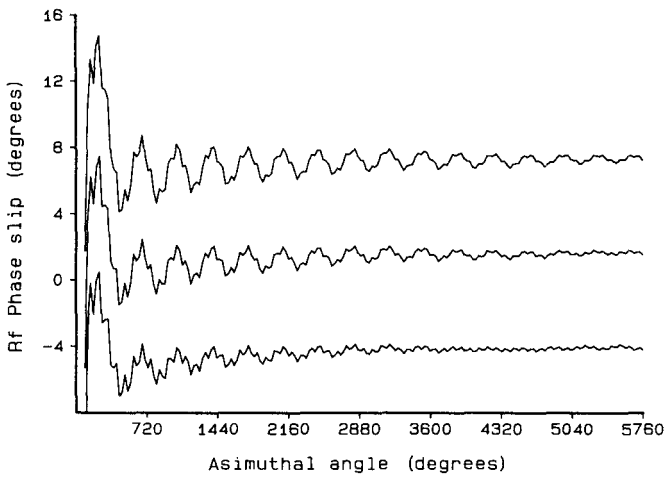

Fig. 3 Phase developement for 8 Mev protons. The middle curve represents the design particle. Particles initially leading or lagging by 7.5 degrees rf are represented by the upper and lower curves respectively.

8 MeV protons is illustrated for the design particle as well as for particles initially lagging or leading by 7.5°, the desired phase acceptance being 15°.

The electrolytic tank used to measure the potential fields employed in modelling the rf fields is described elsewhere[6]. A 3:1 scale model of the central region of SPC1 permitted measurements up to radii of 167 mm. Potential fields of the area limited to the ion source-puller region were carefully measured on a 0.5 mm × 0.5 mm mesh. Fields measured on a 1 mm × 1 mm grid were used in orbit calculations up to radii of 135 mm only, in order to minimise edge effects. These fields also served to determine the values of the two parameters of a Gaussian-type form factor for an analytic model of the electric field employed outside the model limits. In fig. 4 the potential values along a line in the median plane perpendicular to the acceleration gap are shown, together with the derived electrical field values and the analytic fit.

Off the median plane the axial component of the rf field was calculated using the equation $E_z = -z(\partial E_x/\partial x + \partial E_y/\partial y)$. Since E_z contains second derivatives of the potential, it provides a sensitive test for extraneous noise in the data, and also imposes stringent requirements on the accuracy of the measurements. In fig. 5, $z.(\partial E_x/\partial x + \partial E_y/\partial y)$ is plotted for z = 10 mm in the static field of fig. 6 along the 8 MeV proton orbit.

Taking the time dependence of the rf field into account, the noise observed in fig. 5(a) at 1.25 turns (i.e. behind the puller in dee 1) is insignificant.

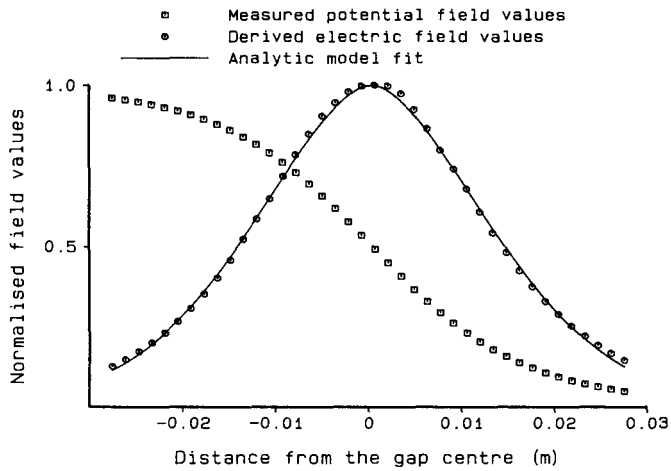

Fig. 4 Fit of the analytic model to the electric field values derived from measured potential values. In all three cases, the maximum value has been normalised to 1.0 .

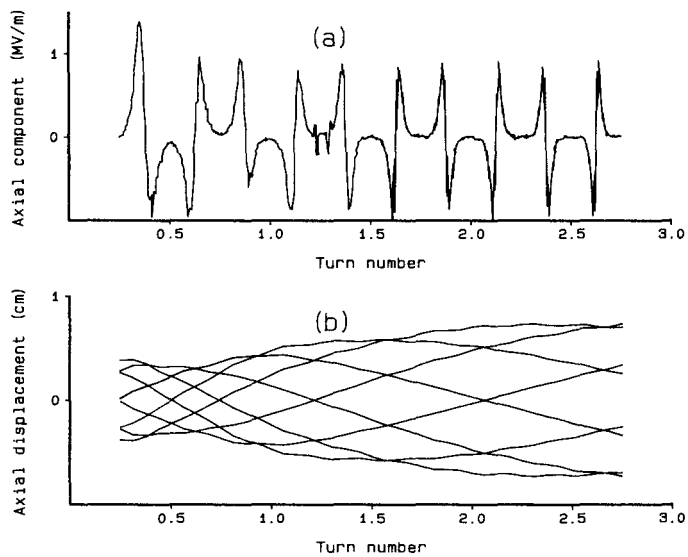

Fig. 5 (a) Axial component of the rf field, 10 mm above the median plane along the 8 MeV design orbit, as derived from a measured potential grid (the time modulation has been suppressed). (b) Motion, in the above field, of 8 particles symmetrically arranged around the circumference of an axial eigenellipse.

4. Ion Source Positions

The optimum rf starting phase at the ion source was determined in the fine mesh field for each CGO. The optimum phases, defined as resulting in the maximum energy gain across the puller gap, was determined from fig. 7 to be -36°, -28°, and -66° for the respective

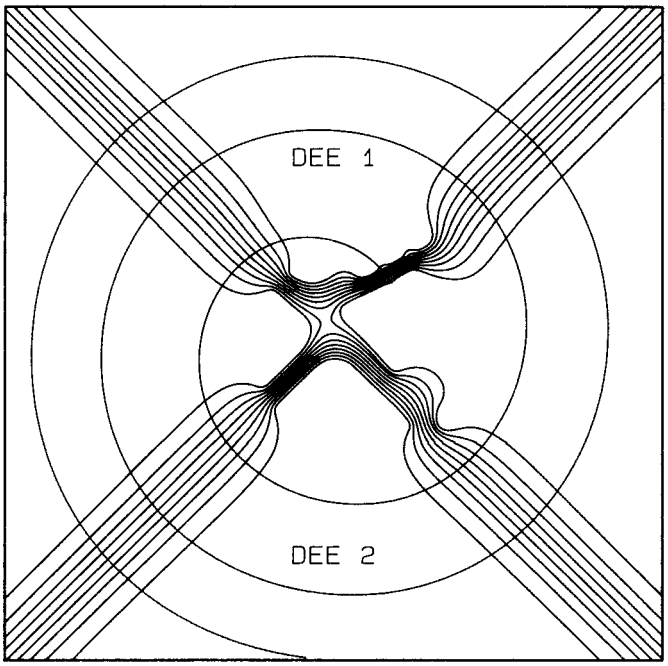

Fig. 6 Equipotential contour map of the measured field for an 8 MeV p constant geometry orbit. The contours are plotted at 10% intervals. The figure shows the entire 270 mm x 270 mm grid, and has the same orientation as fig. 1.

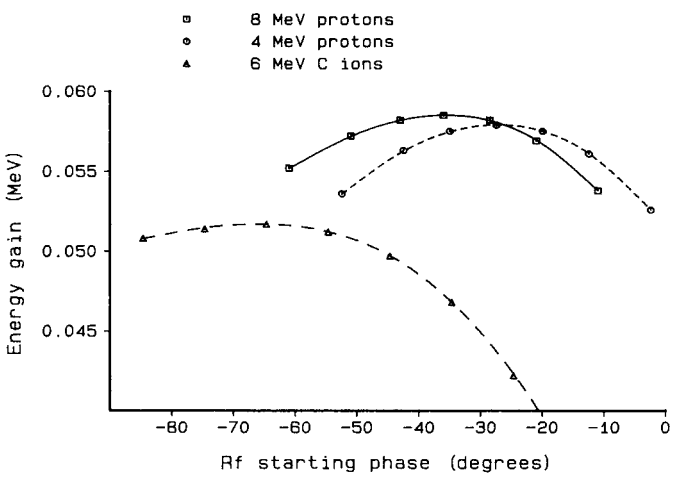

Fig. 7 Energy gain across the puller gap as a function of starting phase. The maxima of the least-squares fitted curves define the optimum starting phases. Note that in the case of the 6 MeV carbon ions, the energy has been scaled by a factor of 1/3.

CGO's. In the third case we decided to use -50^{o} as design phase in order to ensure adequate extraction efficiency at lower dee potentials, i.e. for low-energy light heavy ions. This choice of phase also produced the maximum energy gain at the second gap crossing on CGO3. Orbits of particles starting with the optimum phases were then calculated in the fine mesh fields up to 90^{o} in the first dee. Well-centered orbits, calculated at approximately half the extraction energy, were followed upstream to 90^{o} in the first dee, at the exit of the puller channels. At this point energy matching was searched for by adjusting the starting energy for the backward integration of the centered orbits. Points of matching phase and energy were then found on the two trajectories to be joined. These orbits were thereafter matched in position and momentum at 90^{o} (in the middle of the first dee) by translation and/or rotation of the fine mesh fields encompassing the ion source-puller combination. The results were checked by following the CGO's out from the optimised ion source positions in the transformed fields, and then in the full fields. The design width of the puller gap is 6 mm, and the maximum dee voltage will be 60 kV. The puller slits are 3 mm x 6 mm, 6 mm x 12 mm, and 3 mm x 12 mm (width x height) respectively for the three CGO's. The ion source slit diameter is 3 mm, flared at an angle of 45^{o}.

5. Axial Focusing

Orbit calculations using the initial 3:1 scale model indicated a nett axial defocusing at the second gap crossing on CGO1. It was found that this is due to the proximity of the orbit to the central pillars (fig. 1). This led to several changes being made to the model. In each case the field was measured and the effect of the change checked by orbit calculations. A previous report[2] indicated that improved axial focusing in the central region is obtained by using a magnetic cone field and decreasing (within limits) the gap height. All orbit calculations were now carried out in cone fields. Our results showed that decreased gap heights on entering and leaving a gap improved axial focusing, but that this can be further improved by decreasing the gap height on the entrance side only. The effect this has on the electrical field can clearly be seen from the gap to the left of dee 1 in fig. 6. In this case the entrance height has been reduced from 30 mm to 20 mm to cover the first turn of CGO1 only. The radial extent of the central pillars on the dees and dummy dees was reduced. This also improved the focusing. A further enhancement of the axial focusing was obtained in the gap on the right of dee 2. A small pillar was placed on the dummy dee lip in such a way that it is closer than the central pillar on dee 2 to the fourth gap crossing on CGO1. The effect of the electrical field was found to be dominant for CGO1 up to the 5th gap crossing. After the 5th crossing, the detailed geometry of the central region rf field did not show any marked influence on the axial motion. The electrical focusing is in any case decreasing rapidly with increasing particle energy. On the first few gap crossings the design particle phase is not optimal for axial focusing. As a result of this, leading phases have stronger, but lagging phases weaker, axial focusing.

6. Phase and Momentum Selection

Two radial slits will provide momentum, and a measure of phase selection. A pair of axial slits will be used to further enhance phase selection. For best results, the first slit of each pair should intercept the beam as soon as possible. This also alleviates the problems associated with cooling the slit jaws. The combined first radial and axial slits (fig. 1) is situated in the left dummy dee. The tantalum jaws and water-cooled copper carriers are electrically isolated. The second radial slit, 90^{o} downstream, being in the second dee where space is at a premium, will have to be cooled by conduction to the dee plate by a much longer thermal path. The second axial slit will be situated downstream, separated from the first by half a period in ν_z. The only available space for this slit is in the dummy dee containing the ion source, and to the right of the ion source (fig. 1). In the case of CGO3 the calculated and available positions coincide within 1^{o}. For CGO2, ν_z will have to be fine-tuned from 0.193 to 0.196 to make up the 16^{o} difference in azimuthal angle. The worst case is for CGO1, where ν_z will have to be detuned from 0.122 to 0.110 in order to bring about an

CH1996-3/84/0000-069 $1.00 © 1984 IEEE

azimuthal change of 162°. If the second slit is not half a period of ν_z from the first, orbit calculations indicate that axial beam oscillations may occur.

The axial acceptance as a function of starting rf phase at the ion source was calculated taking into account all gaps up to extraction. The results for 8 MeV protons are given in fig. 8. All gaps and slits were

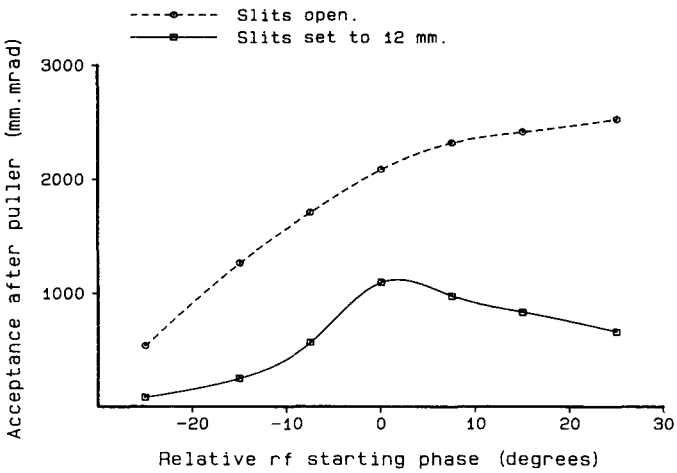

Fig. 8 Axial acceptance for 8 MeV protons, showing the effect of the two axial selecting slits. Phases are given relative to the design particle phase.

projected onto the first axial slit. The selection on the leading relative phases is seen to be weak. Calculating the radial acceptance, excluding the extraction elements, is a much more difficult proposition. In order to obtain a measure of the radial acceptance, an assumption as to the emittance of the beam has to be made, since the emittance of the ion source is not known. We assumed the relative position (X_r) spread as defined by the puller slit width. The relative spread assumed for the momentum (P_r) is illustrated by the inset in fig. 9 for CG01. In this case the acceptance was also limited by the central pillars, especially in the case of particles starting ahead of the design phase.

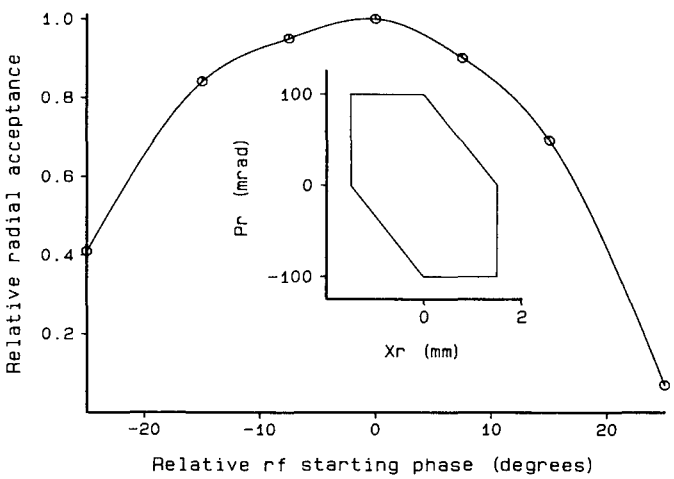

Fig. 9 Radial acceptance for 8 MeV protons, with slits set at 4 mm (40 mm.mrad emittance at extraction). The inset shows the assumed emittance at the puller slit. Refer to text.

Calculations were made to determine the radial momentum selection which could be achieved using the two radial slits. The slits, separated by 90 degrees azimuthally, are a quarter of a period apart in ν_r. Fig. 10 shows the projections of the jaws of the second slit onto the first slit for various settings relative to the design orbit position. The projections for the design particle orbit, as well as for particles leading or lagging in phase by 7.5 degrees, were found by following particles upstream from the second to the first slit by orbit calculations. From this figure one may read off the momenta selected by the second slit, and once this slit has been set, determine the acceptance of the combination for various settings of the first slit.

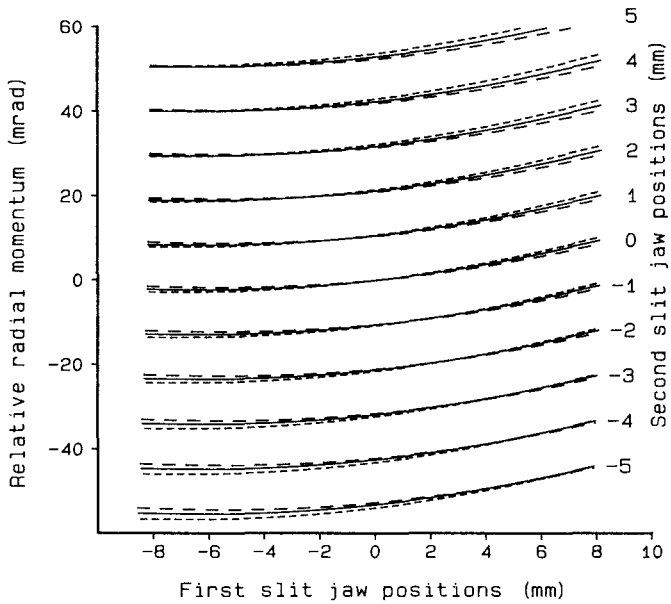

Fig. 10 Projections of the second radial-slit jaws onto the first slit. Jaw positions are given relative to CG01. The solid curves are the projections using the design particle phase. The curves consisting of short(long) dashes are the projections for a 7.5 degree leading(lagging) phase.

References

1. A.H. Botha et al., Proc. 9th Int.Conf. on Cyclotrons and their Applications, (Caen, 1981) p.33.

2. Z.B. du Toit et al., Proc. 9th Int. Conf. on Cyclotrons and their Applications, (Caen, 1981) p.129.

3. M. Reiser, Nucl. Instr. Meth. 18, 19, 370 (1962).

4. Z.B. du Toit et al., Calculated and Measured Magnetic Fields for the Injector Cyclotron at the NAC. This conference.

5. P.M. Cronje, Orbit Code OC (Unpublished).

6. S.J. Burger et al., The Electrolytic Tank Facility at the NAC. This conference.